

# Increasing Temporal Resolution in Greenland Ablation Estimation Using Passive and Active Microwave Data

Ivan S. Ashcraft and David G. Long

Brigham Young University Microwave Earth Remote Sensing Laboratory  
459 Clyde Building, Provo, UT 84602, e-mail: isa2@et.byu.edu, long@ee.byu.edu

**Abstract**—Increasing the accuracy of melt estimation using microwave instruments by focusing on sub-day time scales is addressed. Three Special Sensor Microwave Imager (SSM/I) instruments operating simultaneously over the summer of 2002 are combined to estimate brightness temperature ( $T_b$ ) over daily cycles. Normalized radar cross-section ( $\sigma^\circ$ ) measurements from SeaWinds on QuikSCAT are employed to provide similar estimates of  $\sigma^\circ$  daily variation. The estimates are compared with automatic weather station temperatures. The combination of these measurements provides an increased understanding of the diurnal melt cycle over Greenland and estimation of the melt profile.

## I. INTRODUCTION

Accurate estimation of the mass balance of the Greenland ice sheet is important for predicting sea-level variations related to global climate change. A key component in determining mass balance is ablation (melt). The vast extent of the Greenland ice sheet combined with its harsh climate make it impractical to obtain sufficient in situ data to estimate ablation on an ice sheet wide scale. Studies have demonstrated microwave sensors' ability to detect the extent and duration of melt across the ice sheet. However, current methods use estimates obtained by averaging measurements over a period of a day or more. During the summer varying degrees of melt cause large fluctuations in surface microwave properties over short sub-day periods, adversely affecting the estimate accuracy.

This paper addresses increasing the accuracy of melt estimation by focusing on diurnal variations brightness temperature ( $T_b$ ) normalized radar cross-section ( $\sigma^\circ$ ) measurements. A simple model of the melt process is used to characterize the melt profile using the varying frequency and polarization sensitivities of  $T_b$ . The results are applicable for improving the accuracy of ablation estimates derived from microwave instruments for use in Greenland mass balance studies and global climate analysis.

## II. BACKGROUND

The sensitivity of radiometers and scatterometers to snow melt stems from the dramatic effect the presence of liquid water has on the microwave properties of the snow. For  $T_b$ , the introduction of liquid water causes a large increase in the emissivity ( $e$ ) of the snow,

$$T_b = eT$$

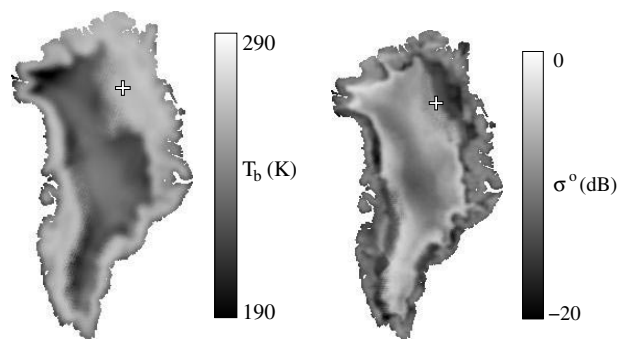


Fig. 1. Greenland SSM/I 19V  $T_b$  (left) and QuikSCAT h-pol  $\sigma^\circ$  (right) images from JD 195, 2002 with study location (78 N, 34 W) indicated with a “+”.

where  $T$  is the actual temperature of the surface in degrees Kelvin. The emissivity remains relatively constant over time for frozen snow, making  $T_b$  approximately a linear function of  $T$  for a given snow surface with a  $T < -7^\circ\text{C}$ . When a melt event occurs there is a large increase in  $e$  resulting in a corresponding increase in  $T_b$ . This is illustrated in the  $T_b$  image of Fig.1 where the periphery of the Greenland ice sheet exhibits high  $T_b$  values. This image is from Julian Day (JD) 195, 2002, a day when the melt is particularly strong in northeast Greenland.

$\sigma^\circ$  also changes dramatically with the introduction of liquid water in the snow. As little as 0.5 percent liquid water increases the conductivity of the surface by over an order of magnitude [1]. This decreases the penetration depth and increases the absorption of the surface with the end result being a significant reduction in  $\sigma^\circ$ . In the QuikSCAT  $\sigma^\circ$  image in Fig. 1 melt is indicated by a dark region between the inner ice sheet and the coastal region.

## III. DATA

The SSM/I instrument is a bi-polar multi-frequency microwave radiometer which measures  $T_b$  using seven channels including 19 GHz vertical polarization (19V), 19H, 22V, 37V, 37H, 85V, and 85H. SSM/I instruments operated aboard the F-13, F-14, and F-15 satellites simultaneously during summer 2002 with their orbits resulting in different time of day observations for each instrument. SeaWinds on QuikSCAT is a Ku-band scatterometer which measures the normalized radar cross-section ( $\sigma^\circ$ ). The SeaWinds instrument has two beams: the inner-beam is horizontally polarized with an incidence

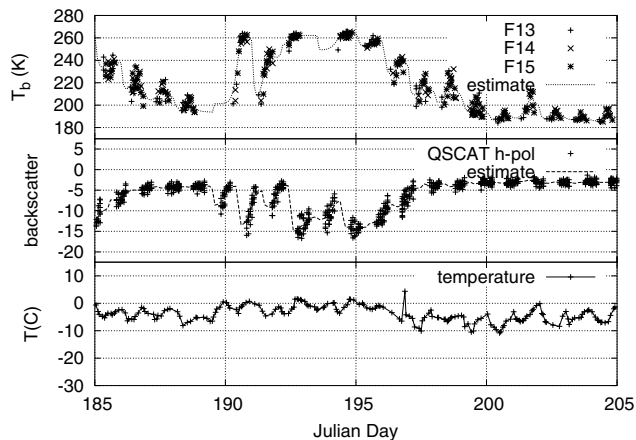


Fig. 2. Raw 19V  $T_b$  and h-pol  $\sigma^o$  measurements from 78.0 N, 34.0 W during the summer of 2002. The lines plotted with raw data show a non-parametric fit to the  $T_b$  and  $\sigma^o$  data. The bottom plot displays near-surface air temperature measurements at the same location.

angle  $\sim 46^\circ$ , and the outer-beam is vertically polarized with an incidence angle  $\sim 54^\circ$ .

Automatic weather station (AWS) near-surface air temperature measurements obtained from the Greenland Climate Network are used to assist in validating melt as the primary contributing factor driving the rapid large fluctuations of the microwave measurements.

The study area is centered at 78.0 N, 34.0 W (see Fig. 1). Microwave measurements with a center within 20 km of this location are included in the analysis. This location was chosen for three primary reasons. First, it is the location of the Tunu-N AWS, so temperature measurements are available. Second, moderate melt is observed in this area during the summer of 2002. Third, no major gaps in the temporal coverage exists for  $\sigma^o$ ,  $T_b$ , or AWS temperature over the primary time interval.

#### IV. MELT CYCLE OBSERVATIONS

A daily freeze/thaw cycle is clearly observed in the raw microwave data sets. Figure 2 shows 19V  $T_b$  and h-pol  $\sigma^o$  measurements during the period JD 185 to 205, 2002 versus time. The Greenwich Mean Standard (GMT) times from the raw data set have been converted to Greenland local time.

Histograms of the pass times for SSM/I and QuikSCAT are shown in Fig. 3. Ascending and descending passes combine to form a continuous 12 hour span of sample times for each sensor type. The typical split between ascending and descending measurements is missing due to the high latitude of this study area, combined with the orbit inclination angle of the satellites. SSM/I measurements occur primarily during the middle of the day when the largest amount of melt is expected to occur. Because of temporal overlap between the three SSM/I sensors, a portion (2100-0600) of each day is not observed. Conversely, QuikSCAT measurements occur over the night period during the refreeze process. The combination of SSM/I and QuikSCAT sampling times cover the complete day, providing insights necessary in understanding the daily

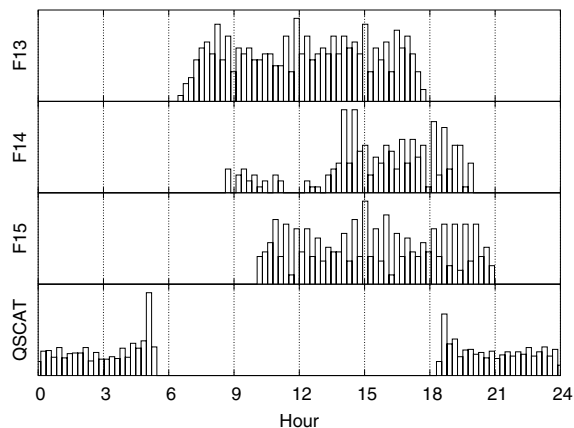


Fig. 3. Histograms of the pass times of the different satellites for the data used in this study. The pass times are local Greenland time.

melt cycle.

Melt is clearly indicated in the data in Fig. 2. On the morning of JD 190, there is a jump of over  $60^\circ$  in  $T_b$  attributed to an increase in the liquid water content of the snow surface associated with a melt event. High  $T_b$  readings persist over a large portion of this 20 day period, indicating persistent melt.

A key component of Fig. 2 is the diurnal variations in the  $T_b$  and  $\sigma^o$  data. Each day there is an observed increase in  $T_b$  as the morning progresses toward mid-day. Similarly,  $\sigma^o$  progresses from a low-value indicating melt to a higher value indicating some refreezing is taking place as evening progresses toward morning. The period between JD 196 and 200 is indicative of a gentle refreeze. The increased spread in the raw data during this period is attributed to spatial inhomogeneities in the refreeze process.

The AWS Temperature data ( $T_{air}$ ) concurs with the microwave data set in indicating periods of melt. During the period from JD 190 to 196 when the melt is most significant,  $T_{air}$  hovers around freezing. After JD 196,  $T_{air}$  drops below freezing as the microwave measurements gently migrate to their frozen state. Figure 4 illustrates the strong relationship between the microwave measurements and  $T_{air}$ . The effects of melt are observed in the 19V  $T_b$  measurements at  $T_{air}$  values as low as  $-10^\circ$  C. By  $-2^\circ$  C, the effects of the melt on  $T_b$  saturate at around  $260^\circ$  K. On the other hand, the  $\sigma^o$  values do not begin to decrease until  $T_{air}$  reaches approximately  $-7^\circ$  C. A melt saturation point for  $\sigma^o$  is not observed in the data. Overall, it appears clear that Ku-band h-pol  $\sigma^o$  is less sensitive to small amounts of melt than is 19V  $T_b$  and correspondingly does not saturate as quickly.

Some care is required in interpreting Fig. 4. Discrepancies are expected between  $T_{air}$  and the actual surface temperature. Surface temperature change is primarily driven by radiation and conduction whereas convection plays a major role in local air temperature change. This is expected to be a contributing factor to the horizontal spread of the observed step in  $T_b$  and  $\sigma^o$  associated with a melt event. Also,  $T_b$  and  $\sigma^o$  measurements are obtained during different stages in the melt cycle. The

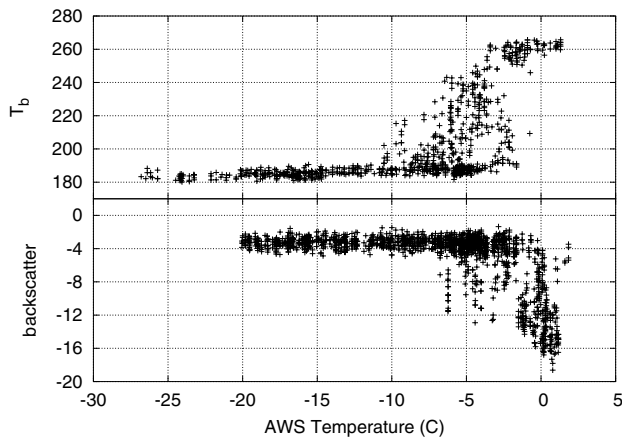


Fig. 4. Scatter plots showing the relationship between  $T_{air}$ ,  $T_b$ , and  $\sigma^o$  at 78 N, 34 W. The  $T_{air}$  values are interpolated from the raw data set to match the satellite measurement times. Data from JD 184 to 236, 2002 are included with measurements from JD 205 to 211 discarded due to the lack of  $T_{air}$  measurements during this period.

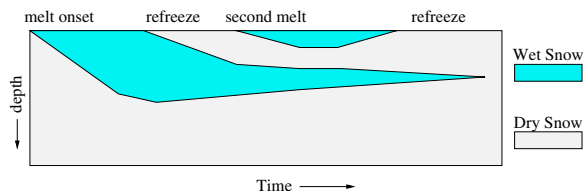


Fig. 5. A simplified illustration progression of the melt profile over time.

surface is generally melting during the  $T_b$  measurements and freezing during the  $\sigma^o$  measurements.

## V. MELT PROFILE

A simplified illustration of the melt cycle is shown in Fig. 5. Initially, melt occurs at the surface. As warm temperatures persist, melting penetrates downward. When temperatures decrease due to nightfall or other factors, the refreezing begins at the surface penetrating downward. If a new melt begins before total refreeze has occurred, a layered melt profile develops.

Both surface and subsurface melting contribute to a large emissivity resulting in high  $T_b$  measurements. However, different polarizations and frequencies respond slightly different to the stages of a melt event. Figure 6 shows various SSM/I channel  $T_b$  ratios. The first and second plot from the top focus on frequency difference, the third and fourth illustrate polarization dependencies, and the bottom plot is another form of the cross-gradient polarization ratio (XPGR) used by Abdalati and Stephen [2] to detect melt. The ratio method has the advantage of eliminating the change in surface temperature and focusing on only differences in emissivity for the two channels.

Variations in the frequency dependence of emissivity aid in detecting periods during which subsurface melt is present under a refrozen surface. The 19V/37V and 19H/37H plots in Fig. 6 are significantly higher during the period between JD 195 and 200 which is a refreezing period. During mid-day when surface melt is most likely, the frequency ratios

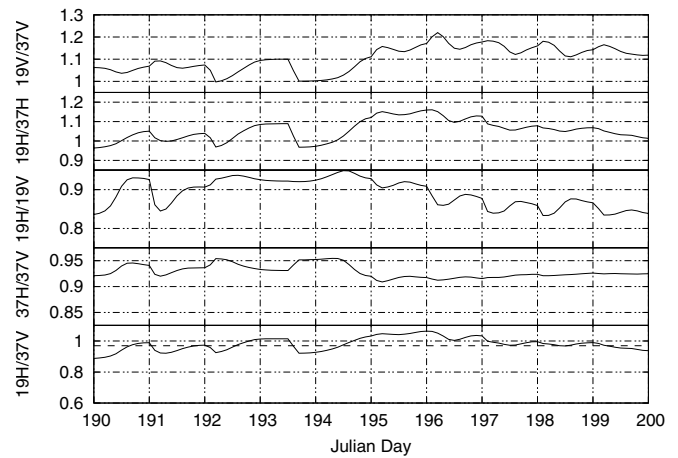


Fig. 6. Ratios of various SSM/I channels brightness temperature valuable in characterizing the melt profile of the surface. Data is for the study point 78 N, 34 W.

move closer to one. This is because the penetration depth of wet snow for both frequencies is virtually zero so that both channels are “seeing” the same snow. However, in dry or refrozen snow the penetration depth at 37 GHz is significantly less than at 19 GHz. Thus, at 37 GHz the refrozen surface is a greater contributor to the signal than at 19 GHz so that the 37 GHz emissivity drops becoming more like that of refrozen snow while the 19 GHz emissivity reduces more slowly due to the effects of the subsurface moisture.

In the polarization ratio plots of Fig. 6 the periods during which surface melting is present are clearly evident. The h-pol  $T_b$  are always less than the v-pol  $T_b$  measurements. However, when surface melting is present the two emissivities become closer to equal. This is clearly evident in the 19H/19V signal during the period JD 190 to 195 when the polarization ratio is closer to one. During the peak melt period from mid-day through evening when surface melting is expected to be present, the polarization ratio is at its maximum value. The late night and morning polarization ratios are lower due to the refreeze occurring at the surface. The bottom plot of Fig. 6 shows SSM/I 19V/37H which provides a compromise between the frequency and polarization ratios in that it is sensitive to both surface and subsurface melt.

Overall, increasing the temporal resolution of  $T_b$  and  $\sigma^o$  data aids in matching data trends to melt cycle processes. This is particularly true for multivariate data sets such as SSM/I  $T_b$  measurements. The data trend/melt process relationship can be applied to distinguish multi-day periods of increasing melt from periods of refreezing. Ablation studies can increase accuracy using custom melt detection criteria based on the melt profile of interest.

## REFERENCES

- [1] F. Ulaby, R. Moore, and A. Fung, *Microwave Remote Sensing: Active and Passive*. Norwood, Massachusetts: Artech House, Inc., 1986, vol. 2.
- [2] W. Abdalati and K. Steffen, “Snowmelt on the Greenland ice sheet as derived from passive microwave satellite data,” *Journal of Climate*, vol. 10, pp. 165–175, February 1997.